Determination of the percentage of magnetite in iron oxide nanoparticles: A comparison between Mössbauer spectroscopy and Raman spectroscopy

Thomas Girardet, Sebastien Diliberto, Cédric Carteret, Franck Cleymand, Solenne Fleutot

Determination of the percentage of magnetite in iron oxide nanoparticles: a comparison between Mössbauer spectroscopy and Raman spectroscopy.

Thomas Girardet[1], Sébastien Diliberto[1], Cédric Carteret[2], Franck Cleymand[1], Solenne Fleutot[1*]

1: Institut Jean Lamour, CNRS, Université de Lorraine, F-54000 Nancy, France
2: Laboratoire de Chimie Physique et Microbiologie pour les Matériaux et l'Environnement, CNRS, Université de Lorraine, F-54500 Vandoeuvre les Nancy

* Corresponding author: solenne.fleutot@univ-lorraine.fr

Abstract

Nanomaterials and especially iron oxide nanoparticles become more common for several fields such as data storage or biomedical applications. For these biomedical applications, iron oxide nanoparticles with a superparamagnetic state are the most used as cancer treatment, contrast agent for MRI… To obtain a superparamagnetic state, the iron oxide must be less than 20 nm in size. It exists several types of iron oxide with a superparamagnetic behaviour: magnetite (Fe_3O_4) and maghemite (γ-Fe_2O_3). For the biomedical fields, the magnetic behaviour must be maximal, therefore the iron oxide synthesised in a preferential way is magnetite. A microwave process is carried out because this synthesis allows to obtain monodisperse nanoparticles with a narrow size distribution and a good crystallinity. However, the quantity of magnetite in our samples is not known exactly. The goal of this study is to determine the amount of magnetite in our samples. The most accurate technique to determine the proportion of magnetite is Mössbauer spectroscopy. A study of our samples with this technique is carried out and is compared to another technique which is Raman spectroscopy. In this work, iron oxide nanoparticles synthesised with a microwave process are characterized by Transmission Electronic Microscopy, X-Ray Diffraction, magnetic measurements, Mössbauer spectroscopy and Raman spectroscopy.

Keywords: iron oxide nanoparticles, microwave process, superparamagnetism, Mössbauer spectroscopy, Raman spectroscopy

1. Introduction

Since few years, nanoparticles are more and more used in the daily life, especially iron oxide nanoparticles in a lot of fields such as depollution [1], energy storage [2], audio loudspeakers [3], printers, dampers [4], biomedical applications [5–10]. For these applications, iron oxide nanoparticles must have a particular magnetic state: the superparamagnetic state. A particle in a superparamagnetic state has no magnetization at room temperature without an applied magnetic field. To obtain a superparamagnetic state with iron oxide nanoparticles, the size must be lower than 20 nm for a spherical nanoparticle without dipolar interactions [11]. This diameter is often called

critical diameter D_C and is depend of the temperature, the volume of the particle and the experimental measuring time [12,13]. Thanks to the superparamagnetic state, Superparamagnetic Iron Oxide Nanoparticles (SPIONs) are used in medical fields for therapy [7,9] (for example hyperthermia), for diagnostic [5,10] (for example contrast agent for Magnetic Resonance Imaging like Endorem®, Lumirem® but they are no longer on the market) or both [6,8]. To synthesise SPIONs, it exists several methods with their advantages and disadvantages. The commonly used are thermal decomposition and coprecipitation [14–19]. With the thermal decomposition, SPIONs obtained are monodisperses, with a narrow size distribution and a good crystallinity [14,15]. However, SPIONs are stable in an organic solvent: another step is mandatory to redisperse SPIONs in an aqueous solution for biomedical applications [20–22]. The other commonly used synthesise is coprecipitation. This synthesis allows to obtain SPIONs directly stable in an aqueous solution. In addition, the conditions to obtain SPIONs are easy: a mix between two iron salts (iron III and iron II) is realised in presence of a basis [17,18]. To increase the dispersion of SPIONs in an aqueous solution and their stability, a ligand is added to solution. This ligand often used are polymer as PVA Poly Vinyl Alcohol) [23], PEG (Poly Ethylene Glycol) [24], … or small molecules as citric acid [19]. For this study, citric acid has been chosen because, thanks to the carboxylate groups, the ligand had a preferential attached to the iron oxide core. With this organic layer, the surface oxidation of the inorganic core is limited [25,26]. Indeed, the synthesis of these nanoparticles allows to obtain magnetite Fe_3O_4. This iron oxide has the high magnetization saturation and allows to have the best magnetic conditions for the used in MRI. If magnetite is oxidised, *i.e.,* Fe^{2+} ions present on the magnetite structure becomes Fe^{3+}, magnetite converts to maghemite γ-Fe_2O_3. Maghemite has the same cubic crystallize structure than magnetite but has some vacancies which decrease the lattice parameter (from 0.8395 nm for the magnetite to 0.8354 nm for the maghemite) [27]. But, the magnetisation saturation of maghemite is smaller than that of magnetite [28]. For magnetite nanoparticles in an aqueous solution, even if there is an organic layer to protect the inorganic core, some oxidation is occurred: iron oxide is sub stoichiometric magnetite $Fe_{3-\delta}O_4$ with δ the deviation from stoichiometry. The range of δ is from 0 to 0.66, i.e. from a structure of magnetite (Fe_3O_4) without oxidation to a structure of maghemite (γ-Fe_2O_3) with a total oxidation of Fe^{2+} to Fe^{3+}. However, it is difficult to determine exactly this value of δ with due to the size of the particles, the structure (core@shell structure or a mixture of magnetite and maghemite) with classical techniques [29]. In our case, thanks to the organic layer, the composition of the synthesise SPIONs corresponds to a mixture of magnetite and maghemite.

To determine δ, some techniques like XPS, XMCD, Mössbauer spectroscopy are often used: with these techniques, the determination of δ can be obtained but after a long time [30–32]. To avoid this inconvenience, the used of another technique such as Raman spectroscopy can be proposed [33,34]. Indeed, a Raman analysis is carried out in few minutes, and it is possible to distinct magnetite to maghemite [35]. But the determination of the the value of δ is very difficult. In addition, a possible oxidation of Fe^{2+} can be induced by the exposure time and the power of the laser [36]. Thus, the goal of this study is to determine the percentage of magnetite in our SPIONs with a comparison between Mössbauer spectroscopy and Raman spectroscopy. For that, SPIONs are synthesised by a microwave process and characterised by some techniques as Transmission Electronic Microscopy to determine the size and the shape, X-Ray Diffraction to justify the crystal structure, Mössbauer spectroscopy and Raman spectroscopy to determine the quantity of magnetite.

2. Materials and methods

2.1. Materials

Ferrous chloride ($FeCl_2 \cdot 4H_2O$) and ferric chloride ($FeCl_3 \cdot 6H_2O$) were purchased from Alfa Aesar. Citric acid ($C_6H_8O_7$) and ammonium hydroxide solution (NH_4OH) were purchased from Sigma Aldrich. In all experiments, ultrapure water (resistivity = 18.2 MΩ·cm) was used.

2.2. Synthesis

A mixture of ferrous chloride ($FeCl_2.4H_2O$; 5.03 mmol) and ferric chloride ($FeCl_3.6H_2O$; 3.70 mmol) are solubilized in 15 mL of ultra-pure water in a pyrex reactor for microwave synthesis. Then, citric acid ($C_6H_8O_7$; 3.16 mmol) is added to the solution and solubilized. Before the microwave heating, 5 mL of ammonium hydroxide is added to precipitate the solution. The reactor is placed on a single mode microwave operates at a frequency of 2.45 GHz (Monowave 400 from Anton Paar). For this study, three different syntheses are studied: one synthesis is heated to 96°C for 40 minutes (called SPIONs_CA1), another is heated to 100°C for 35 minutes (called SPIONs_CA2) and the last is heated to 110°C for 40 minutes. The temperature is controlled by an external infrared sensor.

After the heating, the solution is collected and washing by centrifugation. The first is a centrifugation with absolute ethanol at 10 000 rpm during 5min. Then, another step by centrifugation at 10 000 rpm during 5 min is realised with a mixture between absolute ethanol and ultra-pure water. Finally, a part of the SPIONs collected are redispersed in ultrapure water for TEM analysis. The other part is evaporated at 60°C to obtain a powder for XRD, Mössbauer and Raman analysis.

2.3. Characterizations

2.3.1. Transmission Electronic Microscopy

Transmission Electronic Microscopy (TEM) is used to analyse the shape, the size and the dispersion of nanoparticles on the solvent. TEM is a CM200-FEI operating at 200 kV with a point resolution of 0.27 nm. The size distribution is calculated using free software ImageJ.

2.3.2. X-Ray Diffraction

X-Ray Diffraction (XRD) patterns were recorded in standard conditions with an INEL CPS120 equipped with a monochromatic cobalt radiation (Co K_α = 0.178886 nm) at grazing angle of incidence simultaneously on 120°.

2.3.3. Magnetic characterizations

A Superconducting Quantum Interference Device (SQUID) with a Vibrating Sample Magnetometer (VSM) head is carried out to determine the magnetic properties of the different samples (magnetization saturation M_S and blocking temperature T_B). The magnetic field applied for these measurements sweeps from +5 T (1 T = 10 000 Oe) to -5 T and then from -5 T to +5 T. Thanks to this measurement, the magnetic state and the value of M_S can be determined.

For T_B, a Zero Field Cooled – Field Cooled (ZFC-FC) curve is carried out. The sample is cooled from ambient temperature to 5 K without magnetic field. Then, at 5K, a magnetic field of 0.02 T is applied and the temperature heats to 300 K: the magnetic moment is recorded to give the ZFC curve. Finally, the sample is cooled down from 300 K to 5 K with the same magnetic field: the magnetic moment is recorded too to give the FC curve.

2.3.4. Mössbauer spectroscopy

^{57}Fe Mössbauer spectra are obtained at 300 K and at 4 K in a transmission geometry and constant acceleration mode. The velocity scale was calibrated with a ^{57}Co in Rh matrix radioactive source and a metallic iron foil. The deconvolution of the Mössbauer spectra was performed by the least-square fitting of lines using the Winnormos (Wissel) program.

2.3.5. Raman spectroscopy

Then Raman spectra were collected on a Renishaw in Via^{TM} Qontor^{TM} microspectrometer equipped with a confocal microscope and an Olympus X50 objective (N.A. = 0.55). A 532 nm exciting radiation was used with a laser power below 0.1 mW for all samples to prevent their degradation. The spot area was of few μm^2. Several locations were probed on each sample. The spectral resolution was about 4 cm^{-1} and the precision on the wavenumber was about 1 cm^{-1}.

3. Results and discussions

Figure 1 shows the TEM micrographs of SPIONs_CA1, SPIONs_CA2 and SPIONs_CA3 (respectively figure 1.a, 1.c and 1.e). For all samples, nanoparticles are isolated, without (or a little) aggregation. For the three samples, the size distribution is narrow compared to a size distribution of a classical coprecipitation (figure 1.b, 1.d and 1.f). The mean diameter is equal to 2.6 ± 0.6 nm for SPIONs_CA1, 3.3 ± 0.9 nm for SPIONs_CA2 and 3.5 ± 1.0 nm for SPIONs_CA3. The microwave synthesis allows to control the diameter of iron oxide nanoparticles and to obtain monodisperses SPIONs.

To determine the crystal structure and confirm the presence of magnetite or maghemite, XRD patterns are carried out (figure 2). For the three samples, the mean peaks of magnetite are present.

However, magnetite and maghemite crystallize in the same cubic structure (inverse spinel with the space group $F_{d\bar{3}m}$): the mean peaks of magnetite are like the mean peaks of maghemite. One difference between a magnetite pattern and a maghemite pattern is the position of these peaks. Indeed, the lattice parameter of magnetite is higher to the lattice parameter of maghemite (8.395 Å for magnetite and 8.354 Å for maghemite): there is therefore a shift of the maghemite pattern towards the high angles compared to a magnetite pattern. Due to the size of the different SPIONs, the diffraction peaks are large and does not allow to determine the exact composition of our samples. The lattice parameter of each sample is equal to 0.8384 nm, 0.8388 nm and 0.8370 nm for SPIONs_CA1, SPIONs_CA2 and SPIONs_CA3 respectively: these different lattice parameters are between this of magnetite and this of maghemite. XRD patterns confirm that our samples are sub stoichiometric magnetite $Fe_{3-\delta}O_4$.

Another information obtained with XRD patterns is the crystallite size. Indeed, thanks to the Debye-Scherrer formula, the size of the crystallite can be calculated. For nanoparticles with a small size like our sample, only one single domain composed the nanoparticle: the crystallite can be assimilated to one nanoparticle. To calculate this crystallite size, the mean peak (311) of pattern is used. The crystallite size is equal to 3.5 nm for SPIONs_CA1, 3.8 nm for SPIONs_CA2 and 4.1 nm for SPIONs_CA3: these different crystallite sizes are close to the diameter obtained by TEM measurements. However, due to the using of the Debye-Scherrer formula and the different approximations, the crystallite size obtained is higher than the size obtained with TEM.

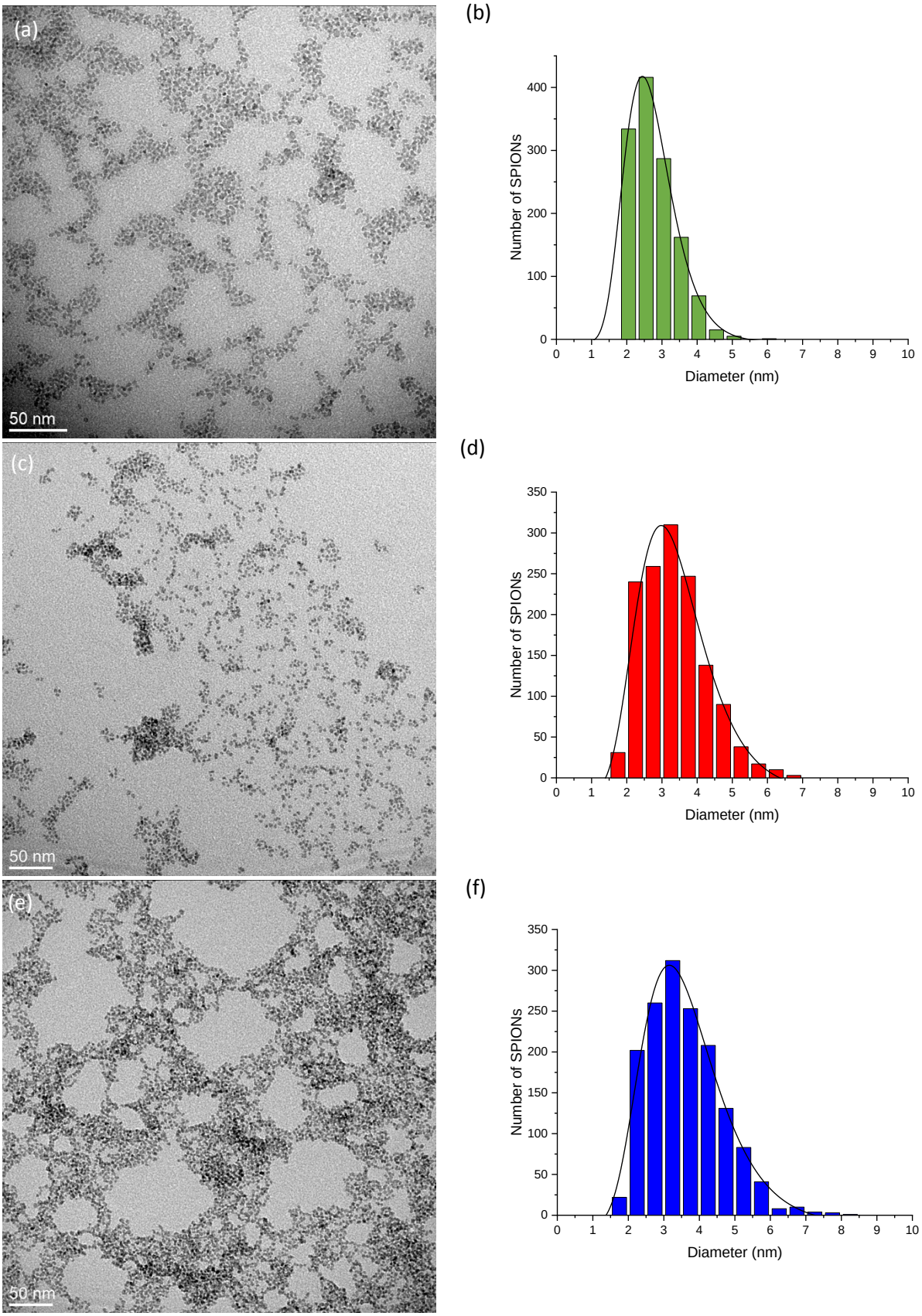

Figure 1: TEM images of SPIONs_CA1 (a), SPIONs_CA2 (c) and SPIONs_CA3 (e) with their size distribution respectively in (b), (d) en (f) fitting by a log-normal function.

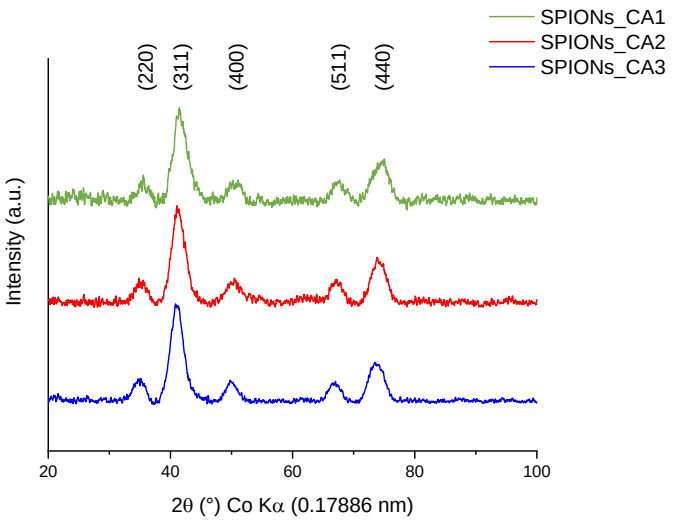

Figure 2: XRD patterns of SPIONs_CA1 (green), SPIONs_CA2 (red) and SPIONs_CA3 (blue) with a cobalt radiation (0.17886 nm)

To determine the magnetic state, several magnetic characterizations are carried out. The first characterization is to determine the magnetization saturation M_S. Figure S1 (in Supplementary Information) shows the magnetic cycle of SPIONs_CA1, SPIONs_CA2 and SPIONs_CA3 at 300 K. For the three samples, no hysteresis is present confirming thus the presence of the superparamagnetic state. The value of each M_S is equal to 55 emu.g^{-1} for SPION_CA1, 53 emu.g^{-1} for SPIONs_CA2 and 59 emu.g^{-1} for SPIONs_CA3: these different values are in the same order than to the M_S of SPIONs with the same diameter [10,37]. To check the transition between the superparamagnetic state to a blocked state, another magnetic cycle is carried out at 5K (Figure S2). At this temperature, a hysteresis is present for each sample, SPIONs are so in a blocked state at low temperature. As the magnetic moment is blocked, the M_S values at 5K are higher than to the values at 300 K. The different M_S are equal to 78 emu.g^{-1}, 78 emu.g^{-1} and 75 emu.g^{-1} for SPIONs_CA1, SPIONs_CA2 and SPIONs_CA3 respectively. To determine the transition temperature between the superparamagnetic state and the blocked state, called T_B, a ZFC-FC measurement is carried out (Zero Field Cooled/Field Cooled). Figure S3 shows the different ZFC-FC curves of the samples. To determine the value of T_B, the maximum of the ZFC curve is taken (the curve from 5 K to 300 K). The maximum of each curve is equal to 14K, 15K and 46K for SPIONs_CA1, SPIONs_CA2 and SPIONs_CA3 respectively: these temperatures confirm the superparamagnetic state at room temperature.

To determine the percentage of magnetite in a sub stoichiometric magnetite, Mössbauer spectroscopy is carried out. The first measurements are recorded at room temperature (figure 3). For the three samples, a doublet is present and corresponding to the superparamagnetic state [38–40]. Indeed, at 300 K, due to the Neel relaxation and the Brownian motion, it is difficult to obtain resolved magnetic hyperfine splitting [41]. Thanks to the presence of the superparamagnetic doublet, the isomer shift (IS) and the electrical nuclear quadrupole moment (EQ) can be calculated and are reported for the three samples on table 1.

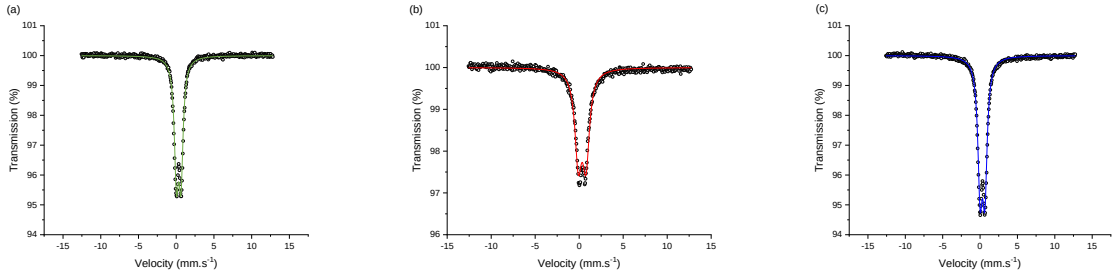

Figure 3: Mössbauer spectra of SPIONs_CA1 (a), SPIONs_CA2 (b) and SPIONs_CA3 (c) at 300K

Table 1: Hyperfine parameters of Mössbauer spectra recorded at 300K.

Sample	Nature	IS ($mm.s^{-1}$)	EQ ($mm.s^{-1}$)	B (T)	Area (%)
SPIONs_CA1	Doublet	0.3335	0.5961	-	100
SPIONs_CA2	Doublet	0.3404	0.8706	-	100
SPIONs_CA3	Doublet	0.3296	0.6293	-	100

At 4 K, below to the blocking temperature T_B, the contribution of divalent and trivalent iron can be identified, separated, and quantified: there are more information on Mössbauer spectra at this temperature (figure 4). Indeed, the magnetic state is in a blocked state at this temperature and did not attenuate the chemical and crystal environment of each iron ions. Thanks to the absence of the superparamagnetic state, the determination of the quantity of magnetite can be operate. As magnetite crystallises in an inverse spinel structure, divalent iron are present in octahedral sites and trivalent iron are present in octahedral and tetrahedral sites: the crystallographic formula of magnetite is $(Fe^{3+})_A[Fe^{2+}Fe^{3+}]_B(O^{2-})_4$ with A the tetrahedral sites and B the octahedral sites. In addition, at this temperature, the behaviour of trivalent iron in octahedral and tetrahedral sites are similar (green line on figure 4). However, for SPIONs_CA1 and SPIONs_CA2, a superparamagnetic contribution is always present (black curve on figure 4): this contribution is due to the presence of SPIONs with a very small size (below to 2 nm). Indeed, the blocking temperature depends on the diameter of the inorganic core: the smaller of size, the lower of T_B.

Thanks to the different contributions of each iron ions, the percentage of magnetite can be calculated: it is equal to 64% for SPIONs_CA1, 65% for SPIONs_CA2 and 54% for SPIONs_CA3. The different Mössbauer parameters are summarised on table 2.

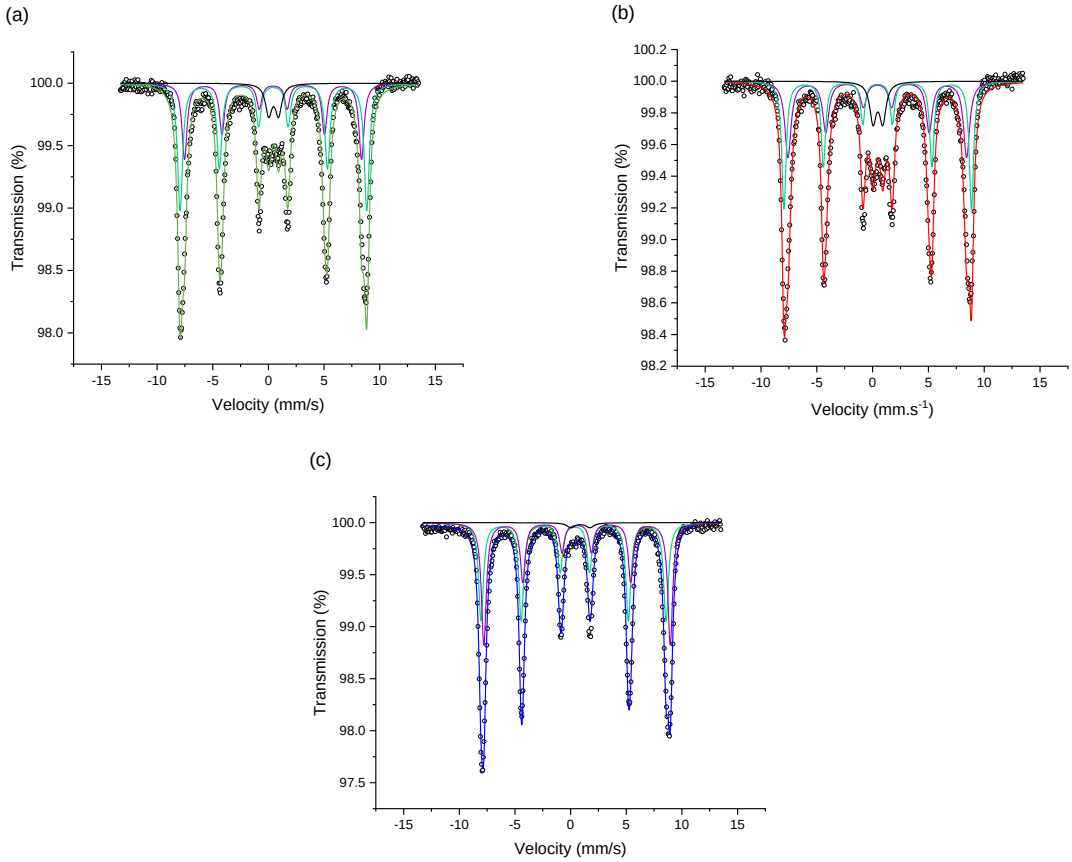

Figure 4: Mössbauer spectra of SPIONs_CA1 (a), SPIONs_CA2 (b) and SPIONs_CA3 (c) recorded at 4K

Table 2: Hyperfine parameters of Mössbauer spectra recorded at 4K.

Sample	Nature	IS ($mm.s^{-1}$)	EQ ($mm.s^{-1}$)	B (T)	Area (%)
SPIONs_CA1	Sextet	0.42	0.00	49.3	33
	Sextet	0.45	0.00	52.0	56
	Doublet	0.47	0.88	-	11
SPIONs_CA2	Sextet	0.43	0.00	49.6	47
	Sextet	0.45	0.00	52.0	40
	Doublet	0.48	0.88	-	13
SPIONs_CA3	Sextet	0.32	0.11	51.6	53
	Sextet	0.57	0.02	52.0	45
	Doublet	-0.17	1.10	-	2

With Mössbauer spectroscopy, the determination of the quantity of magnetite is precise. However, the time of a measurement is long. An alternative to obtain the percentage of magnetite in a sample of iron oxide nanoparticle is Raman spectroscopy. Indeed, the vibrational bands of magnetite are different to the vibrational bands of maghemite because γ-Fe_2O_3 has some vacancies in its crystal structure. Magnetite has three vibrational bands at 310 cm^{-1} (E_g), 540 cm^{-1} (T_{2g}) and the more intense

at 670 cm^{-1} (A_{1g}) [33, 41]. For the maghemite, the different bands are present at 350 cm^{-1} (T_1), 512 cm^{-1} (E) and the strongest at 720 cm^{-1} (A_1) [29–32]. For our samples, the Raman spectra are shown on figure 5 with a comparison of a commercial magnetite. For the three samples, the presence of the three more and less intense bands confirm the presence of magnetite. For each SPIONs, the A_{1g} band is larger compared to the magnetite A_{1g} band: this increase in bandwidth corresponds to an oxidation of divalent iron to trivalent iron in octahedral sites. Thus, thanks to this spilt of the A_{1g} band, a quantification of magnetite in our samples can be operated.

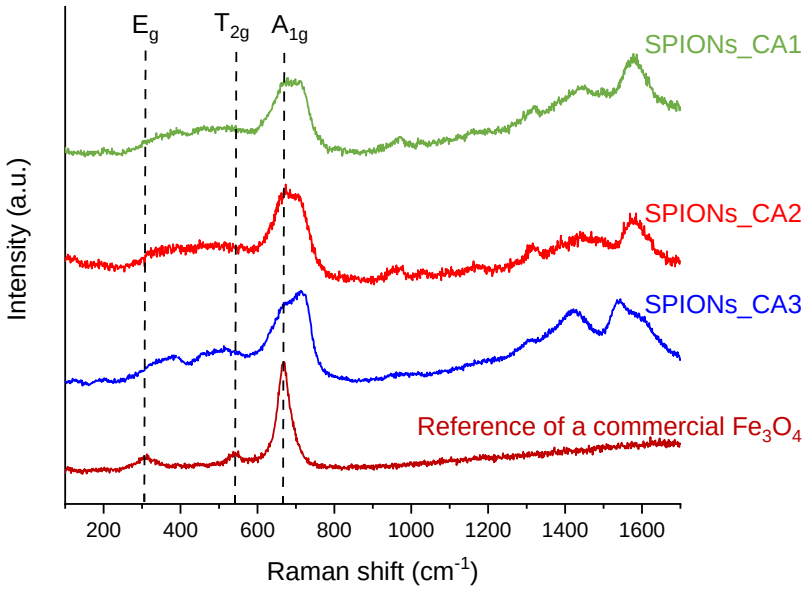

Figure 5: Raman spectra of SPIONs_CA1 (green), SPIONs_CA2 (red) and SPIONs_CA3 (blue) compared to a Raman spectrum of a magnetite reference with a laser at 532 nm.

Figure 6 shows the decomposition of the A_{1g} band for SPIONs_CA1 (figure 6.a), SPIONs_CA2 (figure 6.b) and SPIONs_CA3 (figure 6.c). For the three samples, the band of magnetite at 670 cm^{-1} is more intense than the band of maghemite at 720 cm^{-1}: the percentage of magnetite is higher to the percentage of maghemite. To determine this value, a ratio between the area under the fit curves is realized: the percentage of magnetite is equal to 60% for SPIONs_CA1, 63% for SPIONs_CA2 and 49% for SPIONs_CA3. These values are very close to those obtained with the Mössbauer spectroscopy. So, thanks to the Raman spectroscopy, an estimation of the quantity of magnetite in iron oxide nanoparticles can be made.

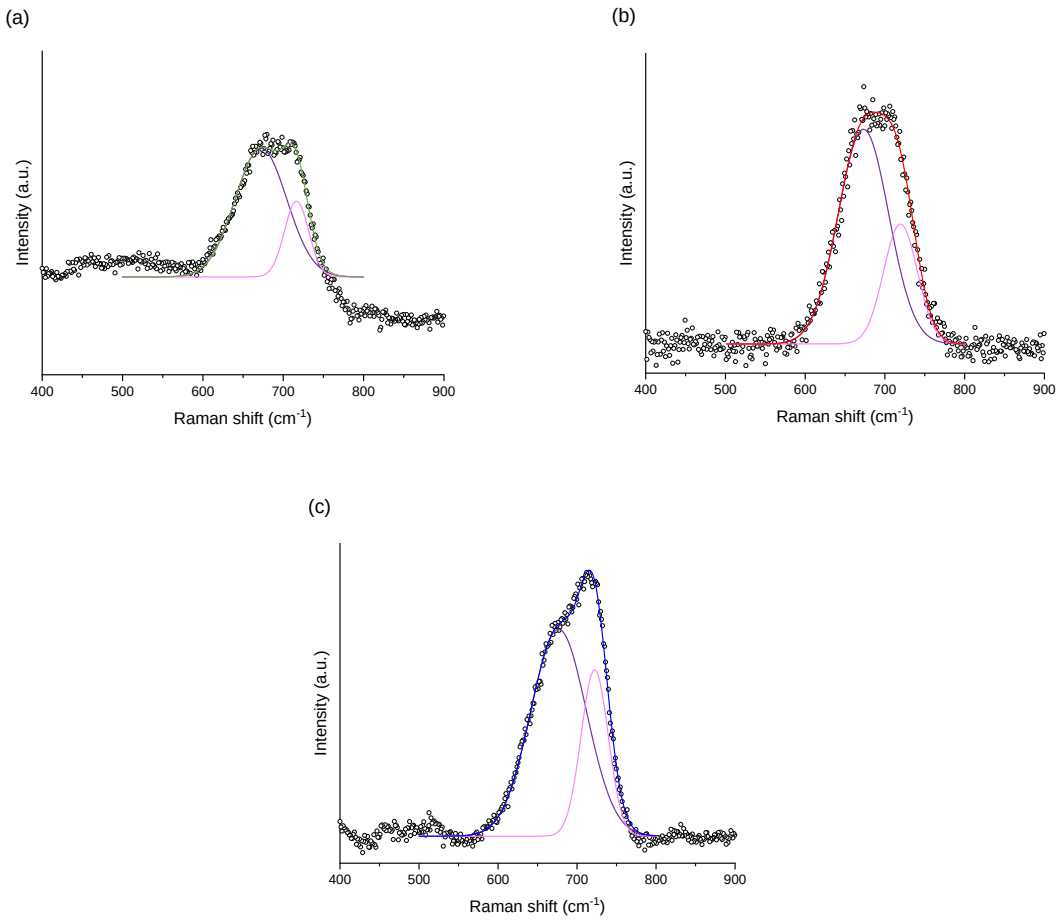

Figure 6: decomposition of the A_{1g} band of the different samples SPIONs_CA1 (a), SPIONs_CA2 (b) and SPIONs_CA3 (c). In purple the band of magnetite at 670 cm^{-1} and in magenta the band of maghemite at 720 cm^{-1}

4. Conclusion

They are more and more syntheses of iron oxide nanoparticles for several fields. The different iron oxide nanoparticles synthesised are essentially magnetite (Fe_3O_4) or maghemite (γ-Fe_2O_3). However, the difference between these two iron oxides is difficult. The goal of this study is to determine in a sample the part of magnetite. Thanks to a microwave process, superparamagnetic iron oxide nanoparticles (SPIONs) are synthesised. Several characterizations are carried out as Transmission Electronic Microscopy to determine the size and the shape, as X-Ray Diffraction to determine the crystallographic structure and as magnetic characterizations to know about the magnetic state at different temperatures. For the different synthesised SPIONs, the diameter is between 2.5 nm and 3.5 nm, they are the same crystallographic structure (an inverse spinel structure) and have superparamagnetic properties at ambient temperature. These different characteristics don't allow to determine the percentage of magnetite in the SPIONs. To overcome that, two techniques allow to quantify the part of magnetite: Mössbauer spectroscopy and Raman spectroscopy. The first is the most used for iron oxide nanoparticles to determine the amount of ferrous ions and ferric ions. Indeed, the magnetic, chemical and crystallographic environment of the different ions in magnetite are different and allow to determine the quantity of divalent and trivalent iron. For our samples, the

quantity of magnetite is equal to 64% for SPIONs_CA1, 65% for SPIONs_CA2 and 54% for SPIONs_CA3. Mössbauer measurements take a long time to acquire. Thanks to the Raman spectroscopy, these amount of Fe_3O_4 can be determined more quickly. Indeed, magnetite and maghemite have different vibrational bands at different Raman shift and the intensity of these bands are proportional to the quantity: the amount of magnetite is equal to 60% for SPIONs_CA1, 63% for SPIONs_CA2 and 49% for SPIONs_CA3. These values are very close to those obtained in Mössbauer spectroscopy.

In conclusion, thanks to the Raman spectroscopy, a determination of the part of magnetite in an iron oxide nanoparticles sample can be realised. However, the percentage of magnetite is not the exact value in the sample: Raman spectroscopy can so give an idea of the amount of magnetite for a screening of a lot of samples and Mössbauer spectroscopy can determine the precise quantity of magnetite. For the next, XPS measurements can be carried out to confirm the percentage of magnetite and a relationship between the percentage of magnetite and the stoichiometric deviation.

Acknowledgements

We would like to acknowledge the spectroscopy and microscopy Service Facility of SMI LCPME for Raman analysis (Université de Lorraine-CNRS– https://www.lcpme.cnrs-nancy.fr).
We would like to acknowledge the center of Microscopy, X-Gamma and Magnetism of Institute Jean Lamour.

Reference

1. K.Q. Jabbar, A.A. Barzinjy, S.M. Hamad, *Environmental Nanotechnology, Monitoring & Management*, 17 (2022) 100661.
2. J. Peng, W. Zhang, L. Chen, T. Wu, M. Zheng, H. Dong, H. Hu, Y. Xiao, Y. Liu, Y. Liang, *Chemical Engineering Journal*, 404 (2021) 126461.
3. S. Galland, R.L. Andersson, M. Salajková, V. Ström, R.T. Olsson, L.A. Berglund, *J. Mater. Chem. C*, 1 (2013) 7963.
4. H. Etemadi, J.K. Buchanan, N.G. Kandile, P.G. Plieger, *ACS Biomater. Sci. Eng.*, 7 (2021) 5432–5450.
5. H. Yang, H. Wang, C. Wen, S. Bai, P. Wei, B. Xu, Y. Xu, C. Liang, Y. Zhang, G. Zhang, *Journal of Nanobiotechnology*, 20 (2022) 1–18.
6. A. Amraee, S. Khoei, M. Bahreyni-Toossi, H. Azimian, F. Ansari, F. Fallahi, N. Robatmili, S. Teshnizi, L. Darvish, *Clinical and Translational Imaging* (2022) 1–9.
7. Y. Luengo, Z.V. Díaz-Riascos, D. García-Soriano, F.J. Teran, E.J. Artés-Ibáñez, O. Ibarrola, Á. Somoza, R. Miranda, S. Schwartz, I. Abasolo, *Pharmaceutics*, 14 (2022) 1526.
8. A. Kader, J.O. Kaufmann, D.B. Mangarova, J. Moeckel, J. Brangsch, L.C. Adams, J. Zhao, C. Reimann, J. Saatz, H. Traub, *Cancers*, 14 (2022) 2909.
9. C. Pucci, A. Degl'Innocenti, M.B. Gümüş, G. Ciofani, *Biomaterials Science*, 10 (2022) 2103–2121.
10. C. Chen, J. Ge, Y. Gao, L. Chen, J. Cui, J. Zeng, M. Gao, *WIREs Nanomed Nanobiotechnol*, 14 (2022).
11. J.L. Dormann, *Advances in Chemical Physisc*, 98 (1997) 283–494.
12. M. Pauly, B.P. Pichon, P. Panissod, S. Fleutot, P. Rodriguez, M. Drillon, S. Begin-Colin, *J. Mater. Chem.*, 22 (2012) 6343.
13. U. Jeong, X. Teng, Y. Wang, H. Yang, Y. Xia, *Adv. Mater.*, 19 (2007) 33–60.
14. Q. Wang, X. Ma, H. Liao, Z. Liang, F. Li, J. Tian, D. Ling, *ACS Nano*, 14 (2020) 2053–2062.
15. C. Xu, S. Sun, *Advanced Drug Delivery Reviews*, 65 (2013) 732–743.

16. S.M. Dadfar, K. Roemhild, N.I. Drude, S. von Stillfried, R. Knüchel, F. Kiessling, T. Lammers, *Advanced Drug Delivery Reviews*, 138 (2019) 302–325.
17. S. Slimani, C. Meneghini, M. Abdolrahimi, A. Talone, J.P.M. Murillo, G. Barucca, N. Yaacoub, P. Imperatori, E. Illés, M. Smari, *Applied Sciences*, 11 (2021) 5433.
18. J. Khanam, M. Ahmed, S. Zaman, N. Sharmin, S. Ahmed, *Bangladesh Journal of Scientific and Industrial Research*, 57 (2022) 67–76.
19. M.S. Yusuf, R. Rahmasari, *Biomedical and Pharmacology Journal*, 14 (2021) 1533–1543.
20. N. Zhu, H. Ji, P. Yu, J. Niu, M. Farooq, M.W. Akram, I. Udego, H. Li, X. Niu, *Nanomaterials*, 8 (2018) 810.
21. F. Crippa, L. Rodriguez-Lorenzo, X. Hua, B. Goris, S. Bals, J.S. Garitaonandia, S. Balog, D. Burnand, A.M. Hirt, L. Haeni, M. Lattuada, B. Rothen-Rutishauser, A. Petri-Fink, *ACS Appl. Nano Mater.*, 2 (2019) 4462–4470.
22. O. Bixner, A. Lassenberger, D. Baurecht, E. Reimhult, *Langmuir*, 31 (2015) 9198–9204.
23. A. Badawi, S.S. Alharthi, M.G. Althobaiti, A.N. Alharbi, *Journal of Vinyl and Additive Technology*, 28 (2022) 235–246.
24. A. Khodadadi, M.R. Talebtash, M. Farahmandjou, *Physical Chemistry Research*, 10 (2022) 537–547.
25. D.K. Kim, M. Mikhaylova, Y. Zhang, M. Muhammed, *Chemistry of Materials*, 15 (2003) 1617–1627.
26. W. Wu, Q. He, C. Jiang, *Nanoscale Research Letters*, 3 (2008) 397–415.
27. M.P. Morales, C. Pecharroman, T. Gonzalez Carreño, C.J. Serna, *Journal of Solid State Chemistry* (1994) 158–163.
28. M.P. Morales, M. Andres-Vergés, M. Veintemillas-Verdaguer, M.I. Montero, C.J. Serna, *Journal of Magnetism and Magnetic Materials* (1999) 146–148.
29. J. Santoyo Salazar, L. Perez, O. De Abril, L. Truong Phuoc, D. Ihiawakrim, M. Vazquez, J.-M. Greneche, S. Begin-Colin, G. Pourroy, *Chem. Mater.*, 23 (2011) 1379–1386.
30. A. Atrei, B. Lesiak-Orlowska, J. Tóth, *Applied Surface Science*, 602 (2022) 154366.
31. M. Thakur, K. De, S. Giri, S. Si, A. Kotal, T.K. Mandal, *J. Phys.: Condens. Matter*, 18 (2006) 9093–9104.
32. S. Brice-Profeta, M.-A. Arrio, E. Tronc, N. Menguy, I. Letard, C. Cartier Dit Moulin, M. Noguès, C. Chanéac, J.-P. Jolivet, Ph. Sainctavit, *Journal of Magnetism and Magnetic Materials*, 288 (2005) 354–365.
33. M. Testa-Anta, M.A. Ramos-Docampo, M. Comesaña-Hermo, B. Rivas-Murias, V. Salgueiriño, *Nanoscale Adv.*, 1 (2019) 2086–2103.
34. M. Hanesch, *Geophysical Journal International*, 177 (2009) 941–948.
35. S.P. Schwaminger, P. Fraga-García, F. Selbach, F.G. Hein, E.C. Fuß, R. Surya, H.-C. Roth, S.A. Blank-Shim, F.E. Wagner, S. Heissler, S. Berensmeier, *Adsorption*, 23 (2017) 281–292.
36. Y. El Mendili, J.-F. Bardeau, N. Randrianantoandro, J.-M. Greneche, F. Grasset, *Science and Technology of Advanced Materials*, 17 (2016) 597–609.
37. M. Basini, T. Orlando, P. Arosio, M.F. Casula, D. Espa, S. Murgia, C. Sangregorio, C. Innocenti, A. Lascialfari, *The Journal of Chemical Physics*, 146 (2017) 034703.
38. C.E. Johnson, J.A. Johnson, H.Y. Hah, M. Cole, S. Gray, V. Kolesnichenko, P. Kucheryavy, G. Goloverda, *Hyperfine Interact*, 237 (2016) 27.
39. R. Gabbasov, M. Polikarpov, V. Cherepanov, M. Chuev, I. Mischenko, A. Lomov, A. Wang, V. Panchenko, *Journal of Magnetism and Magnetic Materials*, 380 (2015) 111–116.
40. S. Sarveena, J.M. Vargas, D.K. Shukla, C.T. Meneses, P. Mendoza Zélis, M. Singh, S.K. Sharma, *Phys. Chem. Chem. Phys.*, 18 (2016) 9561–9568.
41. M. Hanesch, *Geophysical Journal International*, 177 (2009) 941–948.